

1 **SynthETC: A Statistical Model for Severe Winter Storm Hazard on Eastern**  
2 **North America**

3

4 Timothy Hall

5 NASA Goddard Institute for Space Studies

6 New York, NY

7 [timothy.m.hall@nasa.gov](mailto:timothy.m.hall@nasa.gov)

8

9 James F. Booth

10 City College of the City University of New York

11

12

13 **Abstract**

14 We develop, evaluate, and apply “SynthETC,” a statistical-stochastic model of winter  
15 extra-tropical cyclones (ETCs) over eastern North America. SynthETC simulates the  
16 life cycle of ETCs from formation to termination, and it can be used to estimate the  
17 probability of extreme ETC events beyond the historical record. Two modes of  
18 climate variability are used as independent covariates: El Niño/Southern Oscillation  
19 (ENSO) Niño3.4 and the monthly North Atlantic Oscillation (NAO). We use SynthETC  
20 to estimate the annual occurrence rate over sites in eastern North America of  
21 intense ETC passage in different ENSO and NAO states. Positive NAO is associated  
22 with increased rates over the North Atlantic, while negative NAO is associated with  
23 decreased rates over the North Atlantic and increased rates over northern Quebec.  
24 Positive ENSO is associated with decreased rates over the North Atlantic, Ontario,  
25 and the Canadian Maritime, while negative ENSO is associated with increased rates  
26 over those regions, as well as the Great Lakes region.

27

28

29 **1. Introduction**

30

31 Winter extra-tropical cyclones (ETCs) pose a major hazard to eastern North  
32 America. These storms can cause damage through their precipitation, e.g., blizzards  
33 and floods, and through their winds, e.g., extreme surface winds and storm surge.  
34 Heavy snowfall causes power outages, collapse of structures, and suspension of  
35 travel and commerce. ETC winds sometimes reach hurricane force and drive  
36 damaging coastal storm surge. Orton et al. (2016) found that in the New York City  
37 area, ETCs are the dominant cause of surge events that have annual probability  
38 greater than 1%. NOAA's NCDC estimated \$40.9 billion in insured and uninsured  
39 losses due to ETC events from 1980 to 2016 that caused more than one billion  
40 dollars in damage each ([www.ncdc.noaa.gov/billions/summary-stats](http://www.ncdc.noaa.gov/billions/summary-stats); see also Smith  
41 and Katz, 2013).

42

43 ETCs are a dominant source of mid-latitude weather, and their varied formation and  
44 evolution mechanisms have been studied using a wide range of observational,  
45 theoretical, and modeling approaches (reviewed in Catto, 2016). The  
46 characterization of ETC variability in the Northeast US has been documented for  
47 some time (e.g. Miller 1946), and a climatology of northeast ETC tracks exists  
48 (Hirsch et al. 2001). However, our understanding of the link between the storms'  
49 variability, hazardous extreme events, and large-scale climate variability remains  
50 incomplete (Colle et al. 2015). An examination of ETC tracks on seasonal timescales  
51 suggests that there are a large set of forcing parameters, however the variance

52 explained by multiple predictors is less than 50% (DeGaetano 2008).  
53 Climatologically, ETC tracks have been used to identify a preferred track path for  
54 storms that create wind hazards in the northeast (Booth et al. 2015). However, the  
55 probabilistic analysis in that work is limited by the short time span of the reanalysis  
56 utilized. A large body of work on case studies has led to a general appreciation of  
57 snow storms in the region (Kocin and Uccellini, 2002), but the distinction between  
58 these case studies and all other ETC tracks has not been made.

59

60 There has also been work examining the link between ETC paths and planetary scale  
61 climate variability (i.e., teleconnections patterns) for the Northeast region. Eichler  
62 and Higgins (2006) composited track density by phases of El Niño/Southern  
63 Oscillation (ENSO), and Grise et al (2013) composited by ENSO, the North Atlantic  
64 Oscillation (NAO), the Pacific North American pattern (PNA), and the Madden-Julian  
65 Oscillation (MJO) separately. DeGaetano et al. (2002) used a discriminant  
66 forecasting procedure to find heightened ETC activity over the U.S. east coast for  
67 positive ENSO and NAO states. Berhardt and DeGaetano (2012) used seasonal  
68 averages of ETC tracks to show that storm surge is more likely to occur in the region  
69 during ENSO positive years concurrent with NAO negative years. However, the  
70 statistical significance in their analysis is limited by the small number of times those  
71 two events have occurred at the same time for the time period used in the Berhardt  
72 and DeGaetano (2012) study: 1951-2006. Ning and Bradley (2015) found regional  
73 correlations between extreme winter precipitation over the northeastern U.S. and  
74 southeastern Canada and ENSO, the NAO, and the PNA. Their work focused on the

75 precipitation events only, and so there is still a need to explore the three-part link  
76 between the teleconnection patterns, the ETC paths, and the resulting hazards.

77

78 Multiple approaches to understand the connections between storms and hazards  
79 exist, including case-study analysis, numerical modeling, and statistical modeling.  
80 Our work here utilizes statistical modeling. Such an approach has been adopted  
81 widely for tropical cyclones, for both commercial and academic applications (e.g.,  
82 Vickery et al., 2000; James and Mason, 2005; Emanuel et al., 2006; Rumpf, et al.,  
83 2007; Hall and Jewson, 2007; Hall and Yonekura, 2013; Yonekura and Hall, 2014;  
84 Bonazzi et al., 2014). Additionally, a statistical downscaling approach has been  
85 utilized substantially in Europe for windstorms (Klawanda and Ulbrich, 2003; Haas and  
86 Pinto 2012; Born et al., 2012; Seregina et al., 2014), and to a lesser extent in North  
87 America as well (He et al. 2010). While these studies focus on ETC-related hazards,  
88 the statistical models are not built around the cyclone paths or storm tracks. The  
89 statistical modeling of Eulerian storm tracks (Compo and Sardeshmukh, 2004;  
90 Ambaum and Novak, 2014; Yang et al. 2015) helps explain the physics of the storm  
91 tracks on seasonal time scales. However they do not offer distinct information about  
92 ETC tracks. Gaffney et al. (2006) developed regression-mixture models of existing  
93 ETC tracks, and used the models to cluster the tracks based on their trajectory  
94 (regardless of location). The model/cluster analysis was useful for assessing the  
95 skill of a GCM in generating ETC tracks. However, the model was not designed to  
96 generate synthetic ETC tracks. Hunter et al. (2016) used ETC tracks to build an

97 aggregate risk model and found that including both the frequency and intensity  
98 information improved the model skill.

99

100 A major goal of our effort is to quantify the rate of extreme ETC events on local  
101 regions throughout eastern North America, including events that have not occurred  
102 historically. There are various statistical approaches possible. The advantage of a  
103 statistical track model compared to approaches that emphasize local historical  
104 occurrence is that information from the entire domain is exploited for the local rate  
105 estimation. This is particularly valuable for estimating rates for events that have  
106 never occurred historically and/or for estimating rates in combinations of climate  
107 indices for which there are few historical instances. In effect, the large synthetic  
108 event set increases the precision of rate estimates. While the complexity of  
109 generating synthetic storm sets may introduce bias, Hall and Jewson (2008) showed  
110 for tropical cyclones that the gain in precision outweighs the potential loss in  
111 accuracy.

112

## 113 **2. Data**

114

115 The Bauer et al. (2016) cyclone tracking algorithm (MCMS) was applied to 1979-  
116 2015 ERA-Interim reanalysis (Dee et al. 2011) sea level pressure (SLP) data to  
117 generate global ETC tracks based on the position of the ETC central pressure  
118 minimum. ERA-Interim has been shown to be as good or better than other existing  
119 reanalyses for tracking ETCs in the Northern Hemisphere (Hodges et al. 2011). The

120 decision to use data for 1979 onward is based on the improved skill in the  
121 reanalyses in the satellite era.

122

123 A regional subset of the tracks was defined as all tracks that had at least one 6-  
124 hourly position within the region spanning: 110°W by 45°W and 25°N by 65°N.  
125 Using all months of the year, this regional subset contained 12049 tracks. We refer  
126 to these as the “historical” data. They are comprised of 6-hourly values of storm  
127 center position and central pressure. Most of the storms are weak disturbances. We  
128 are most interested in simulating intense ETCs. To this end, we filter the historical  
129 ETCs: 1. We remove tropical cyclones (TCs), by removing tracks that closely match  
130 HURDAT (Landsea et al., 2015), in terms of location of the storm center during the  
131 track evolution; and 2., keep only the remaining ETC tracks whose central pressure  
132 (CP) for at least one point along the track falls 35mb or lower (“35mb+”) than the  
133 local annual-cycle SLP climatological value at that point. We will also refer to these  
134 as strong, or intense, cyclones, and we refer to the CP deficit from local climatology  
135 as the intensity of the storm. To create the climatology, we first create daily data by  
136 averaging the SLP from 00, 06, 12 and 18Z. The daily data is averaged from 1979 -  
137 2015 and then smoothed using a 30-day running mean. This provides a daily  
138 climatological value for SLP at each latitude/longitude location that is subtracted  
139 from the 6-hourly SLP for each cyclone center, providing measure of cyclone  
140 intensity based on the SLP anomaly. The total number of 35mb+ storms is 1782, and  
141 these storms comprise the training dataset for SynthETC. This is a sufficient number  
142 of events for model training, more than twice as many, in fact, as the number of

143 events used successfully in the tropical cyclone model training of Hall and Jewson  
144 (2007).

145

146 MCMS identifies tracks based on the depressions in SLP. But the initial location and  
147 the termination location are primarily determined based on existence of a local  
148 minimum in SLP. The tracker performs as well as alternate existing tracking  
149 algorithms (Bauer et al. 2016), and includes data regarding a region of influence of  
150 each cyclone. However, we here use only the track data. All trackers have some  
151 difficulty detecting cyclones in regions of steep terrain (Neu et al. 2013), and  
152 therefore we do not focus on the area near the Rockies.

153

154 Fig 1 shows the 1979-2015 35mb+ historical ETC tracks; that is, the 1979-2015 ETC  
155 tracks whose CP for at least one point along the track is at least 35mb lower than the  
156 local SLP. Fig 2 shows the monthly histogram of storm frequency for the full set, the  
157 full ETC set (minus TCs), and the 35mb+ ETC set. While the full set has little annual  
158 cycle, the set of intense ETCs strongly peaks in winter, dropping nearly to zero in  
159 summer. This is consistent with the seasonality of the strength of the baroclinicity.  
160 The 35mb value is the approximate minimum threshold that excludes the vast  
161 majority of summer storms.

162

163 The independent variables in our analysis are 1979-2015 monthly time series of  
164 ENSO and NAO. For ENSO we use the monthly Niño3.4 SST index available on  
165 NOAA's ESRL website ([www.esrl.noaa.gov/psd/gcos\\_wgsp/Timeseries/Nino34](http://www.esrl.noaa.gov/psd/gcos_wgsp/Timeseries/Nino34)),



166 which is derived from HadISST1 gridded SST data (Rayner et al., 2003). For the NAO  
167 we use the monthly index available from the Climate Research Unit of the University  
168 of East Anglia ([crudata.uea.ac.uk/cru/data/nao/nao.dat](http://crudata.uea.ac.uk/cru/data/nao/nao.dat)), which is derived from SLP  
169 differences between Iceland and the Azores and Gibraltar (e.g., Jones et al., 1997).

170

### 171 **3. Model**

172

173 In developing SynthETC we aim to model ETC tracks stochastically from formation  
174 through termination. The goal is twofold:

175

176 1. To construct an ETC “event set”, much larger than the historical set, that has  
177 the statistical properties of the historical set. The large synthetic set allows  
178 more precise estimates of rates of rare events than estimates based solely on  
179 the historical storms, and allows estimation of the probability for events that  
180 have not occurred historically.

181 2. To estimate the impact of NAO and ENSO on the occurrence rates of extreme  
182 ETCs. These indices are dominant modes of climate variability, and have  
183 been shown to influence winter ETC frequency (e.g., DeGaetano et al., 2002),  
184 although they are by no means the only factors (Grise et al., 2013; Yang et al.,  
185 2015). Additional covariates could be tested and utilized. However, for  
186 seasonal and longer-term probabilistic hazard modeling (as opposed to a  
187 nearer-term operational modeling) our covariate selection is strongly

188 influenced by parsimony and by the requirement that covariate forecasts be  
189 available for seasonal forecasting.

190

191 SynthETC is based on 37 years of reanalysis track data, 1979-2015. To estimate  
192 return periods of events well beyond 37-years the model assumes that 1979-2015 is  
193 statistically representative of much larger time periods; that is, that the ETC  
194 statistics are stationary. SynthETC provides rates of rare events that haven't  
195 occurred in the historic 1979-2015 record, but would happen eventually if the  
196 1979-2015 period were repeated many times. There is evidence for non-stationarity  
197 in ETC meteorology, for example, an increased frequency and northward shift in the  
198 mean storm track (e.g., Voce et al., 2014). Such signals are not currently included in  
199 SynthETC, though the model could be used to explore the impact of secular changes  
200 in mean track or cyclogenesis rates and locations on extreme storm statistics.

201

202 Our modeling approach is similar to Hall and Jewson (2007) and Hall and Yonekura  
203 (2013) for tropical cyclones. SynthETC consists of four components: 1. formation, 2.  
204 propagation, 3. termination, and, 4. central pressure. Formation, propagation, and  
205 termination are modeled via local regression, while central pressure is modeled  
206 using a weighted sampling scheme. We review the components briefly here, and  
207 refer readers to Hall and Yonekura (2013) for additional methodological details.

208

209 **3.1. Formation**

210 At each point on a  $1^\circ$  by  $1^\circ$  grid, Poisson regression is performed in which the  
211 dependent variable is the monthly number of 35mb+ ETCs originating “near” the  
212 grid point, and the independent variables are monthly NAO and ENSO indices. In  
213 order to focus on cold-season storms we use only the months October through April  
214 in the time series, which capture the vast majority of 35mb+ ETCs (Fig. 2). “Near” is  
215 determined by the Gaussian weighting kernel used in the calculation of the  
216 regression coefficients. The weight of a formation event to the regression declines  
217 with distance from the point according to a Gaussian kernel. The bandwidth of the  
218 kernel (140km) is determined by drop-one-year out-of-sample likelihood  
219 maximization. The result of the regression at each location is a Poisson mean rate  
220 for the number of ETCs formed monthly within Oct-Apr as a function of NAO and  
221 ENSO for the weighted area about the grid point. This rate is then scaled down to  
222 the grid box area by the ratio of the grid-box area to the weighted area under the  
223 kernel. The formation rate dependence on ENSO and NAO is illustrated and  
224 discussed in Section 4.2.

225

226 Once the monthly rates are estimated, seasonality needs to be accommodated, so  
227 that, for example, October rates are appropriately different than January rates for  
228 the same NAO and ENSO values. A kernel pdf in formation location and pentad-of-  
229 year is constructed with optimized bandwidths of 140 km and 15 days. At each  
230 location the pentad-of-year dependence is normalized and then multiplied by the  
231 monthly rate from the Poisson regression at that location, resulting in a pentad  
232 Poisson rate consistent with the date, as well as NAO and ENSO. Fig 3 shows the

233 spatial map of the kernel pdf for the central pentad of each of the 12 months of the  
234 year. The bulk of formation for these intense ETCs occurs in the winter off the US  
235 eastern seaboard, typical of nor'easters. There are also pockets of activity in the  
236 Midwest, particularly over the Great Lakes (Sanders and Gyakum, 1980).

237

238 Formation occurs during simulations as follows: During each pentad of year at each  
239  $1^\circ$ -by- $1^\circ$  site, the ENSO and NAO values for the current simulation month are  
240 combined with the regression coefficients to determine the monthly Poisson rate.  
241 The rate is multiplied by the pentad-of-year pdf for the site, and the resulting  
242 Poisson distribution is sampled to determine how many formation events have  
243 occurred.

244

245 To examine uncertainty in formation ENSO and NAO dependence due to the finite  
246 (37 year) data record we perform a bootstrap analysis on the Poisson regression for  
247 the domain-wide Oct-Apr 35mb+ formation count. The best estimate difference  
248 between the most (ENSO=-2 and NAO=+2 in units of standard deviations) and least  
249 (ENSO=+2 and NAO=-2) active states is 31 storms annually Oct-Apr (60 compared  
250 to 29). The 5%-95% confidence limits on this difference over the bootstrap set is 38  
251 to 23. Thus, while there is considerable uncertainty in the mean rate's ENSO and  
252 NAO sensitivity, the sign of the sensitivity is robust. In future analysis we plan to  
253 perform such bootstrap analysis on all components of the model.

254

255 **3.2. Propagation**

256

257 Tracks are simulated in 6-hour increments. Given a simulated ETC center at position  
258  $\mathbf{x}(t)$  we determine its position at  $\mathbf{x}(t+6hr)$  by analyzing the propagation of “nearby”  
259 (defined below) historical ETCs. A set of 6-hourly latitude and longitude increments  
260 from the historical ETCs is constructed, and these increments are regressed on three  
261 covariates: NAO, ENSO, and an annual cycle of 500mb NCEP winds. The coefficients  
262 resulting from the regression are combined with the current values of the covariates  
263 in the simulation to generate the mean 6-hourly simulation track increment from  
264  $\mathbf{x}(t)$ . “Nearby” is defined by a Gaussian weighting kernel; that is, the contribution of  
265 historical track increments to the regression at  $\mathbf{x}(t)$  declines with distance from  $\mathbf{x}$   
266 according to this kernel. The bandwidth of the kernel, 200 km, is determined by  
267 drop-one-year-out out-of-sample forecast error minimization.

268

269 Treatment of the residuals from the regressions is an important part of the  
270 simulations. It constitutes the stochastic component of the track model. The  
271 residuals are standardized assuming a non-isotropic correlated bi-normal  
272 distribution whose coefficients (x and y variances and co-variances) are calculated  
273 from analysis of nearby historical residuals. Once standardized, the two directions  
274 can be modeled independently as a lag-one auto-regressive process, AR(1), whose  
275 autocorrelation coefficient is calculated from analysis of nearby historical  
276 standardized anomalies. Performing a simulation increment thus consists of  
277 drawing a random normal, obtaining standardized anomalies from the AR(1) model,  
278 dimensionalizing and rotating the anomalies using the variances and co-variances to  
279 obtain residuals, adding the means, and finally updating the position of the

280 simulated track. More details can be found in Hall and Jewson (2007) and Hall and  
281 Yonekura (2013).

282

283 Fig 4 illustrates the track calculation, showing a four-day mean track launched from  
284 an arbitrary point (72°W, 36°N). The figure also shows 1000 tracks launched from  
285 the same point and date, now fully simulated with the stochastic component.  
286 Although the general orientation is similar, there is considerable spread of the  
287 stochastic tracks about the mean track, indicating that much of the track variance is  
288 unexplained by the covariates (ENSO, NAO, 500mb annual cycle winds). The set of  
289 1979-2015 historical tracks that originate near the launch point (shown in blue)  
290 appears as a typical subset of the much larger synthetic set.

291

### 292 **3.3. Termination**

293

294 At each six-hour time step starting at step 6 (1.5 days) of a track simulation a  
295 random number is drawn and compared to a termination probability. If the  
296 probability exceeds the draw, then the track is terminated. The probability,  $P$ , is the  
297 fraction of nearby historical track points that are terminal; i.e.,  $P$  equals the  
298 weighted sum of terminal points divided by the weighted sum of all points, where  
299 the weighting kernel is Gaussian with a 150km bandwidth. The 1.5-day onset of  
300 termination is chosen to mimic the duration distribution of the historical ETCs, for  
301 which 1.5 days is the shortest track. The resulting simulation and historical track-

302 duration frequency distributions match closely, and the mean simulation track  
303 duration is 4.5 days, compared to 4.8 days for the historical set.

304

### 305 **3.4. Intensity**

306

307 Intensity is simulated by weighted random sampling of historical intensity time  
308 series; i.e., time series of SLP local climatology minus CP. Once a track is simulated  
309 we select from the set of historical intensity time series a single time series to place  
310 on the simulated track. The selection is weighted towards historical intensity series  
311 whose associated tracks are “similar” to the simulated track in question. “Similar” is  
312 defined by a set of bandwidths associated with the Gaussian weighting kernels of  
313 the criteria. The criteria are the date of year, duration of track, and locations of track  
314 formation, mid-point, and termination. This scheme results in a selected intensity  
315 time series similar, though not generally identical, in start date and duration to the  
316 simulation track. The intensity series is then shifted and scaled in time to match the  
317 start date and duration of the simulation track. An example of out-of-sample  
318 intensity simulation on a historical track from 2012 is shown in Fig 5 using sampling  
319 data from 1979-2015 that excludes 2012. In this example seven historical intensity  
320 time series have probabilities greater than 0.001 of being selected, with the most  
321 probable having 0.45. During simulations the sampling scheme selects a single time  
322 series, most commonly the series with the highest probability, but sometimes one  
323 with lower probability.

324

325 Hunter et al. (2016) found evidence for a correlation between track density and  
326 intensity, and concluded that much of the relationship was driven by the mutual  
327 dependence of both variables on several modes of climate variability, including  
328 NAO. In our intensity-sampling scheme, dependence of intensity on ENSO and NAO  
329 is indirect. ENSO and NAO influence the formation region and track shape, and  
330 these, in turn, influence the intensity time-series selection. If the physical  
331 relationship between NAO-ENSO and ETCs has a signature in both intensity and  
332 formation or track, then an NAO-ENSO-intensity relationship will be captured by  
333 our sampling scheme.

334

335 Once the weighted random sampling is performed, the lifetime maximum intensity  
336 (LMI) along the track receives a small random perturbation so that simulated LMIs  
337 are not limited to historical values. The perturbations are drawn from a generalized  
338 extreme value fit of the historical LMIs to ensure that the distribution of the  
339 perturbed set conforms closely to that of the unperturbed set.

340

341 In this initial development of the model, we have chosen to use CP deficit with  
342 respect to local SLP as the measure of storm intensity. This is due to its simplicity  
343 and the fact that it is a reasonable proxy for the SLP gradient around the storm,  
344 which drives cyclonic winds. Other measures of storm strength are relative vorticity  
345 at 850 hPa (e.g., Hoskins and Hodges 2002) and the strength of surface winds.  
346 However, with these there is a question of what region around the storm to use, or  
347 what horizontal resolution to consider when calculating the vorticity. Sanders and



348 Gyakum (1980) defined storm intensification based on a change in SLP normalized  
349 to a fixed latitude. Because the focus here is intensity and not intensification, the CP  
350 difference from climatology is used to remove the effects of latitudinal variation in  
351 climatological SLP (see Ulbrich et al. 2009 for more discussion). However, a  
352 relationship between latitude and intensity does exist, with stronger storms  
353 occurring further north. We attribute this primarily to the fact that ETCs in our  
354 study region typically travel north and strengthen during their life cycle, e.g.,  
355 Hoskins and Hodges (2002). There may also be some bias with respect to latitude in  
356 our intensity metric, due to the absence of explicit inclusion of the Coriolis  
357 parameter's dependence on latitude, which affects the geostrophic wind-pressure  
358 relationship. Future work with the model will be dedicated to testing the impact of  
359 different metrics of storm intensity, including synthetic wind fields.

360

#### 361 **4. Simulations and Analysis**

362

363 We perform two classes of simulations: 1. 1000 repeat simulations of the 1979-2015  
364 historical period (37,000 yrs), driven by the historical ENSO and NAO time series;  
365 and 2. 10,000-yr simulations with ENSO and NAO held constant in each of 25  
366 combinations of ENSO = -2, -1, 0, +1, +2 and NAO = -2, -1, 0, +1, +2 in units of  
367 standardized anomalies. The first set is used to evaluate the model against historical  
368 diagnostics and to estimate average occurrence rates of extreme ETC events. The  
369 second set is used to estimate the impact of ENSO and NAO on extreme event  
370 occurrence rates.

371

372 Fig 6 shows tracks from four sample simulations of 1979-2015 and can be  
373 compared to Fig 1. The overall shape and distribution of the historical tracks are  
374 well captured by the simulations. The majority of intense ETCs in the historical data  
375 and the simulations occur over the North Atlantic. However, there are occurrences  
376 of 30mb+ and even 60mb+ intensity extending into the U.S. northeast and Canadian  
377 Maritimes.

378

379 SynthETC provides a way to estimate probabilities of extreme events that are well  
380 beyond the historic record. Fig 7 shows three examples of synthetic ETCs that pass  
381 within 200km of Washington DC, New York City, and Boston with intensity greater  
382 than 60mb, having peak intensities of 71mb, 67mb, and 60mb, respectively.  
383 Frequency analysis of the 37,000-year synthetic set reveals that ETCs with 60mb+  
384 intensity passing within 200km of Boston, New York City, and Washington DC have  
385 average return periods of 96 yrs, 308 yrs, 2018 yrs, respectively. Finally, occurring 8  
386 times in the synthetic set (average return period of 2800yrs) is an ETC with 60mb+  
387 intensity within 200km of all three cities. Such a storm would devastate the US east  
388 coast, shutting down economic activity for many days and potentially causing power  
389 outages for millions of people.

390

#### 391 **4.1. Model Evaluation**

392

393 To evaluate the model we compare values of diagnostics derived directly from the  
394 historical ETCs to the distribution of values derived from the ensemble of  
395 simulations. A necessary condition for a stochastic model to be unbiased is that the  
396 diagnostic value (e.g., track flux across constant longitude lines) derived from the  
397 historical ETC data should be a typical member of the set of diagnostic values from  
398 the simulations. Fig. 8 shows the number of tracks crossing lines of constant  
399 longitude and latitude. For most regions the historical curve falls inside the spread  
400 of simulation curves, consistent with a lack of bias. An exception is at high Arctic  
401 latitudes, where the model underestimates eastward propagation. This region is  
402 outside our primary area of interest.

403

404 To evaluate the model further, we calculate the return periods as a function of  
405 intensity of ETCs passing within 200km of nine US cities: New York New York,  
406 Boston Massachusetts, Washington DC, Toronto Ontario (Canada), Chicago Illinois,  
407 Detroit Michigan, Montreal Quebec (Canada), Halifax Nova Scotia (Canada), and  
408 Duluth Minnesota (Fig 9). The spread of return period curves across the 1000  
409 simulations of 1979-2015 bounds the curve obtained from the historical data in  
410 most regions and intensities, again consistent with a lack of bias. When the  
411 simulations are placed in series, intensity values at return periods beyond the 37-  
412 year duration of the historical data can be estimated. For example, the analysis  
413 indicates that an ETC with intensity greater than 60mb within 200km of New York  
414 is about 308-year event and within 200km of Boston about a 96-year event. (See  
415 also Fig. 7.) Neither such event occurs in the 37-year historical record.

416

## 417 **4.2. ENSO and NAO Dependence**

418

419 We use the model to estimate the dependence of regional extreme ETC annual rate  
420 as a function of ENSO and NAO. The model is run for 10,000 years each for 25 fixed  
421 combinations of ENSO and NAO: ENSO=-2,-1,0,+1,+2 and NAO=-2,-1,0,+1,+2 in  
422 standardized units. The synthetic storms for each multi-year simulation are then  
423 used to compute a map of the annual probability of occurrence within 200km of an  
424 ETC with 50mb+ intensity. Fig 10 shows these spatial maps for nine ENSO-NAO  
425 combinations, and Fig 11 shows the fractional change with respect to the neutral  
426 (0,0) state. Figs 12 and 13 show the effects of NAO-ENSO on ETC formation rates  
427 and tracks separately. These figures illustrate properties of model mean rates that  
428 are well converged due to the large number of simulation years. Uncertainties on  
429 these mean rates due to the choice of the training data and choices in modeling  
430 schemes will be explored in future work.

431

432 Positive NAO is associated with an increased rate of passage of severe ETC (50mb+  
433 intensity) in the North Atlantic (NA) and a decreased rate over the mid-latitude  
434 Atlantic and northern Quebec, and negative NAO is associated with the opposite  
435 (Fig. 11). There is also a smaller region of enhanced ETC passage rate over the US  
436 mid-Atlantic states for positive NAO. The increased NA rate for positive NAO is  
437 consistent with increased formation to the southwest over the Canadian maritime  
438 and Canadian Midwest (Fig 12). However, the increased ETC rate in northern

439 Quebec for negative NAO has no such negative-NAO formation increase to the  
440 southwest. The Quebec increase can, however, be understood in terms of the NAO  
441 influence on tracks. Fig 13 shows mean tracks of fixed duration (16 time steps or 4  
442 days) launched from three points in nine ENSO and NAO combinations. Negative  
443 NAO is associated with slower (i.e., shorter in Fig 13) continental tracks that are  
444 more prone to curve north into northeastern Canada before reaching the NA,  
445 resulting in increased passage in that region. Similarly, tracks originating at lower  
446 latitude are slower and more zonal, and there is an increase in ETC occurrence in  
447 the Atlantic at mid latitudes for NAO negative. By contrast, for positive NAO the  
448 tracks are straighter, northeastward oriented, and faster, enhancing the higher NA  
449 rates (Figs 10, 11).

450

451 The NAO dependence is largely consistent with past studies. Serreze et al. (1997),  
452 Pinto et al. (2009), Grise et al. (2013) and Hunter et al. (2015) examined the effect  
453 on ETCs of the NAO (and other climate modes) using varying domain definitions and  
454 track datasets. All four studies found increased (decreased) NA track density and  
455 decreased (increased) subtropical and mid-latitude Atlantic track density during  
456 positive (negative) NAO, similar to the anomalies of Fig 11. The results here are also  
457 consistent with Gaffney et al (2007), who classified ETC tracks using a clustering  
458 analysis. Gaffney et al (2007) found that northeastward straight and fast tracks  
459 (their “D cluster”) occurred preferentially during positive NAO phases, while the  
460 slower, eastward tracks occurred preferentially during negative NAO phases, similar  
461 to the more southern mean track dependence of Fig 13.

462

463 However, our result of increased rate of severe ETCs over northern Quebec for  
464 negative NAO is at odds with Grise et al. (2013). The reasons for the difference are  
465 unclear, but we note that the metrics are not strictly comparable, as we restrict  
466 attention to extreme storms defined by CP deficit, while Grise et al. uses a surface  
467 relative vorticity threshold. Our negative-NAO northward tracks are reminiscent of  
468 the northward “V cluster” of Gaffney et al (2007), whose preferential SLP anomaly  
469 pattern has some overlap with negative NAO. Serreze et al (1997) also inferred a  
470 positive winter ETC anomaly for negative NAO over northern Labrador and Quebec.  
471 Our result of increased rates over the U.S. upper Midwest and Ontario for low NAO  
472 is consistent with the negative correlation between extreme precipitation and NAO  
473 in that region found by Ning and Bradley (2015).

474

475 ENSO is associated with severe ETC rate anomalies distinct from NAO. Rates are  
476 lower (higher) for positive (negative) ENSO over the NA and northeastern Canada,  
477 reaching into the northeast US and the upper US Midwest. Unlike the northern  
478 Quebec feature for the NAO, the ENSO effects can be explained qualitatively by  
479 anomalies in formation. Positive (negative) ENSO is associated with a swath of  
480 decreased (increased) formation across the US Midwest, northeast and NA that is  
481 upstream of regions of decreased (increased) passage rates (Fig. 12). Compared to  
482 NAO, ENSO has a smaller effect on mean tracks, though there is a shift to more zonal  
483 propagation during positive ENSO (Fig 13) consistent with a more robust zonal jet, a  
484 shift that modifies the spatial distribution of passage rates.

485

486 The ENSO dependence is also consistent with past studies. *Grise et al. (2013)* saw an  
487 increase (decrease) in ETC track density and formation over a swath of area  
488 including the US Midwest, northeast, and the NA for lower (higher) ENSO anomaly.  
489 They also saw the opposite sign effect to the south of this swath, which is hinted at  
490 in our Fig 11 by the small blue (red) patches in the mid-latitude Atlantic indicating  
491 decreased (increased) passage rate for lower (higher) ENSO. (This regional effect is  
492 weaker in our analysis because of the restriction to intense ETCs.) A similar pattern  
493 in track-density was found by *Eichler and Higgins (2006)* and *Plante et al. (2015)*.  
494 *Plante et al. (2015)* in particular observed a distinct increased occurrence of intense  
495 ETCs (by vorticity) over the Great Lakes region for negative ENSO, consistent with  
496 our results in Fig 11. *Ning and Bradley (2015)* also found a negative ENSO-extreme  
497 winter precipitation correlation over the northern Great Lakes region. Finally,  
498 *Degaetano (2008)* observed that El Niño is associated with increased US east-coast  
499 frequency for all winter storms, but that there is little effect for strong storms, again  
500 consistent with our results. Note that track-density and precipitation as a metric is  
501 sensitive to ETC propagation and formation. By contrast, the analysis here isolates  
502 the ENSO influences on formation and propagation, revealing a larger effect via  
503 formation than propagation.

504

505 In some regions ENSO and NAO can combine to increase rates more than either  
506 alone. For the Great Lakes region and northern Quebec the combination of negative  
507 ENSO and negative NAO results in a sharp increase in rate of intense ETC passage.

508 For the New York and southern New England region negative ENSO and positive  
509 NAO maximize the rate. These sensitivities are illustrated in Fig 14 at Duluth and  
510 New York City. Over Duluth there is a factor of eight minimum-to-maximum  
511 variation in annual passage rate of 50mb+ intensity ETCs ( $0.004-0.03 \text{ yr}^{-1}$ ) from  
512 ENSO and NAO = -2, -2 to +2, +2. Over New York City the variation is a factor of four  
513 ( $0.012-0.05 \text{ yr}^{-1}$ ). Berhardt and DeGaetano (2012) found increased US northeast  
514 storm surge occurrence for positive ENSO and negative NAO, a combination that we  
515 find results in a negative extreme ETC rate anomaly in the region. This is not  
516 contradictory, however, because the focus of Berhardt and DeGaetano (2012) was  
517 storm propagation speed. The enhanced surge was associated with slower moving  
518 ETCs, which we see in negative NAO (Fig 13), and which also tend to be weaker.

519

## 520 **5. Conclusions**

521

522 We have developed, evaluated, and applied “SynthETC”, a new statistical-stochastic  
523 model of ETC hazard for Eastern North America. The model simulates the life cycle  
524 of ETCs from formation to termination, using central pressure deficit from local SLP  
525 climatology as the measure of intensity. SynthETC can be used to estimate the rates  
526 of events on local regions, including unlikely but severe events that may not have  
527 occurred in the historical record. Model evaluation shows that SynthETC matches  
528 well (and extends) ETC occurrence statistics on a range of eastern North American  
529 sites. Generation of large synthetic ETC event sets is an approach to winter-storm  
530 hazard assessment that is consistent with hurricane hazard assessment in the



531 commercial catastrophe modeling industry (e.g., Bonazzi et al., 2014). We are  
532 currently working to develop wind fields to go along with the synthetic track and  
533 pressure time series, clearly necessary to translate severe ETC occurrence rates to  
534 wind and storm surge hazard.

535

536 SynthETC uses two key modes of natural climate variability as independent  
537 covariates: ENSO and the NAO. We find regional severe ETC passage-rate  
538 sensitivities to ENSO and NAO that are largely consistent with past studies using  
539 different methodologies. ENSO can be forecast skillfully months in advance. It is  
540 natural to ask, therefore, if SynthETC could be used to make probabilistic seasonal  
541 forecasts of ETC hazard. We are planning tests to determine whether such forecasts  
542 are skillful.

543

#### 544 **Acknowledgements**

545 This work was supported by the NASA IDS grant “Vulnerability of the U.S. Atlantic  
546 Coast to Hazards Associated with Extreme Winter Storms” (NNX14AD48G) and  
547 NASA MAP grant “Subpolar North Atlantic Air-Sea Fluxes Associated with Mid-  
548 Latitude Cyclones and their Effect on AMOC” (NNX15AJ05A).

549

550

551 **References**

- 552 Ambaum, M. H. P. and Novak, L. (2014), A nonlinear oscillator describing storm  
553 track variability. *Q.J.R. Meteorol. Soc.*, 140: 2680–2684. doi:10.1002/qj.2352.
- 554 Bauer, M., G. Tselioudis, and W. B. Rossow, 2016: A new climatology for investigating  
555 storm influences in and on the extratropics, *J. Appl. Meteor. Climatol.*, 55, 1287-1303.
- 556 Bernhardt J. E. and A. T. DeGaetano, 2012: Meteorological factors affecting the speed  
557 of movement and related impacts of extratropical cyclones along the U.S. east  
558 coast, *Nat. Haz.*, **61**, 1463-1472.
- 559 Bonazzi, A. , A. L. Dobbin, J. K. Turner, P. A. Wilson, C. Mitas, and E. Bellone (2014), A  
560 simulation approach for estimating hurricane risk over a 5-yr horizon, *Weather*  
561 *Clim. Soc.*, **6**, 77-90.
- 562 Booth, J. F., H. Reider, D. E. Lee, Y. Kushnir, 2015: The paths of extratropical cyclones  
563 associated with wintertime high wind events in the Northeast United States.  
564 *Journal of Applied Meteorol. and Clim.* **54**, 1871-1885.
- 565 Born, K., P. L. Ludwig, and J. G. Pinto, 2012: Wind gust estimation for mid-European  
566 winter storms: Towards a probabilistic view. *Tellus*, **64A**, 17471,  
567 doi:10.3402/tellusa.v64i0.17471.
- 568 Cato, J. K., 2016: Extratropical cyclone classification and its use in climate studies.  
569 *Rev. Geophys.*, 54, 486-520.
- 570 Colle, B. A., J. F. Booth, E. K. M. Chang, 2015: A review of historical and future  
571 changes of extratropical cyclones and associated impacts along the U.S. east coast.  
572 *Current Climate Change Reports. Current Climate Change Reports* **1**, 125-143.

573 Compo, G. P. and P. D. Sardeshmukh, 2004: Storm Track Predictability on Seasonal  
574 and Decadal Scales. *J. Climate* 17, 3701–3720.

575 DeGaetano, A. T., M. E. Hirsch, and S. J. Colucci, 2002: Statistical prediction of  
576 seasonal east coast winter storm frequency, *J. Clim.*, 15, 1101-1117.

577 DeGaetano, A. T. 2008. Predictability of seasonal east coast winter storm surge  
578 impacts with application to New York's Long Island. *Meteorological Applications*,  
579 15, 231-242.

580 Dee D. P., et al., 2011: The ERA-Interim reanalysis: configuration and performance of  
581 the data assimilation systems. *Quart. J. Roy. Meteor. Soc.*, **137**, 553-597.

582 Eichler, T., and W. Higgins, 2006: Climatology and ENSO-related variability of North  
583 American extratropical cyclone activity, *J. Clim.*, 19, 2076-2093.

584 Emanuel, K., E. Vivant, and C. Risi, 2006: A statistical deterministic approach of  
585 hurricane risk assessment. *Bull. Amer. Meteor. Soc.*, **87**, 299-314.

586 Gaffney, S.J., Robertson, A.W., Smyth, P., S. J. Camargo, M. Ghil, 2007: Probabilistic  
587 clustering of extratropical cyclones using regression mixture models. *Clim Dyn*  
588 29-4 pp 423–440.

589 Grise, K. M., S.-W. Son, and J. R. Gyakum, 2013: Intraseasonal and interannual  
590 variability in North American storm tracks and its relationship to equatorial  
591 Pacific variability, *Mon. Wea. Rev.*, 141, 3610-3625.

592 Hall, T. M., and S. Jewson, 2007: Statistical modeling of North Atlantic tropical  
593 cyclone tracks, *Tellus*, 59A, 486-498.

594 Hall, T. M., and S. Jewson, 2008: Comparison of local and basinwide methods for risk  
595 assessment of tropical cyclone landfall. *J. Appl. Meteor. Climatol.*, **47**, 361-367.

596 Hall, T. M., and E. Yonekura, 2013: North American tropical cyclone landfall and SST:  
597 A statistical model study, *J. Clim.*, **26**, 8422-8439.

598 Haas, R., and J. G. Pinto, 2012: A combined statistical and dynamical approach for  
599 downscaling large-scale footprints of European windstorms, *Geophys. Res. Lett.*,  
600 **39**, L23804, doi:10.1029/2012GL054014.

601 He, Y., A. H. Monahan, C. G. Jones, A. Dai, S. Biner, D. Caya, and K. Winger, 2010:  
602 Probability distributions of land surface wind speeds over North America. *J.*  
603 *Geophys. Res.*, **115**, D04103, doi:10.1029/2008JD010708.

604 Hodges, K. I., R. W. Lee, L. Bengtsson, 2011: A Comparison of Extratropical Cyclones  
605 in Recent Reanalyses ERA-Interim, NASA MERRA, NCEP CFSR, and JRA-25. *J.*  
606 *Climate*, **24**, 4888–4906.

607 Hoskins, B. and K. Hodges, 2002: New Perspectives on the Northern Hemisphere  
608 Winter Storm Tracks. *J. of Atmos. Sci.*, **59**, 1041-1061.

609 Hunter, A., D. B. Stephenson, T. Economou, M. Holland, and I. Cook, 2016: New  
610 perspectives on the collective risk of extratropical cyclones. *Q. J. R. Meteorol. Soc.*,  
611 **142**, 243-256.

612 James, M. K., and L. B. Mason, 2005: Synthetic tropical cyclone database, *J. Waterw.*  
613 *Port Coastal Ocean Eng.*, **131**, 181-192.

614 Jones, P. D., T. Jonsson, and D. Wheeler, 1997: Extension of the North Atlantic  
615 Oscillation using early instrumental pressure observations from Gibraltar and  
616 South-West Iceland, *Int. J. Climatol.*, **17**, 1433-1430.

617 Klawa, M. and Ulbrich, U. 2003: A model for the estimation of storm losses and the  
618 identification of severe winter storms in Germany, *Nat. Hazard Earth Syst. Sci.*, 3,  
619 725–732.

620 Kocin, P. J. and L. W. Uccellini, 2002: Snowstorms along the Northeastern Coast of  
621 the United States, Volume I. *Amer. Meteor. Soc.*, 280 pp.

622 Landsea, C., J. Franklin, and J. Beven, 2015: The revised Atlantic hurricane database  
623 (HURDAT2), NHC NOAA, [nhc.noaa.gov](http://nhc.noaa.gov).

624 Miller, J. E., 1946: Cyclogenesis in the Atlantic coastal region of the United States. *J.*  
625 *Meteor.* **3**, 31-44.

626 Neu, U., and Coauthors, 2013: IMILAST – a community effort to intercompare  
627 extratropical cyclone detection and tracking algorithms: assessing method-  
628 related uncertainties. *Bull. Am. Meteor. Soc.*, 94:529-547, doi:  
629 <http://dx.doi.org/10.1175/BAMS-D-11-00154.1>

630 Ning, L., and R. S. Bradley, 2015: Winter climate extremes over the Northeastern  
631 United States and Southeastern Canada and teleconnections with large-scale  
632 modes of climate variability. *J. Clim.*, 28, 2475-2493.

633 Orton, P. M., T. M. Hall, S. A. Talke, A. F. Blumberg, N. Georgas, and S. Vinogradov,  
634 2016: A validated tropical-extratropical flood hazard assessment for New York  
635 Harbor, *J. Geophys. Res.*, in press..

636 Pinto, J. G., S. Zacharias, S., A. H. Fink, G. C. Leckebusch, U. Ulbrich, 2009: Factors  
637 contributing to the development of extreme North Atlantic cyclones and their  
638 relationship with the NAO. *Clim. Dyn.*, **32**, 711–737.

639 Plante, M., S.-W. Son, E. Atallah, J. Gyakum, and K. Grise, 2015: Extratropical cyclone  
640 climatology across eastern Canada, *Inter. J. Clim.*, **10**, 2759-2776.

641 Rayner, N. A., D. E. Parker, E. B. Horton. C. K. Folland, L. V. Alexander, D. P. Rowell, E.  
642 C. Kent, and A. Kaplan, 2003: Global analysis of sea surface temperature, sea ice,  
643 and night marine air temperature since the late nineteenth century, *J. Geophys.*  
644 *Res.*, **108** (D14), 4407, doi:10.1029/2002JD002670.

645 Rumpf, J. H. Weindl, P. Hoppe, E. E. Raughe, and V. Schmidt, 2007: Stochastic  
646 modeling of tropical cyclone tracks. *Math Methods Oper. Res.*, **66**, 475-490.

647 Sanders, F. and J. R. Gyakum, 1980: Synoptic-Dynamic climatology of the "bomb".  
648 *Mon. Wea. Rev.*, **108**, 1589-1606.

649 Seregina, L. S., R. Haas, K. Born, J. G. Pinto, 2014: Development of a wind gust model  
650 to estimate gust speeds and their return periods. *Tellus A* **66**, 22905.  
651 doi:10.3402/tellusa.v66.22905

652 Serreze, M. C., F. Carse, R. G Barry, and J. C. Rogers, 1997: Icelandic low cyclone  
653 activity: climatological features, linkages with the NAO, and relationships with  
654 recent changes in the Northern Hemisphere circulation. *J. Climate*, **10**, 453-464.

655 Smith, A. B., and R. W. Katz, 2013: US billion-dollar weather and climate disasters:  
656 data sources, trends, accuracy and biases, *Natural Hazards*, **67**, 387-410.

657 Ulbrich U, Leckebusch GC, Pinto JG (2009) Extra-tropical cyclones in the present and  
658 future climate: A review. *Theor Appl Climatol*, **96**,117–131

659 Vickery, P., P. Skerij, and L. Twisdale, 2000: Simulation of hurricane risk in the U.S.  
660 using empirical track model, *J. Struct. Eng.*, **126**, 1222-1237.

661 Vose, R.S., et al. 2014: Monitoring and understanding changes in extremes: extratropical  
662 storms, winds, and waves. *Bulletin of the American Meteorological Society* 95:377-  
663 386, doi:10.1175/BAMS-D-12-00162.1.

664 Yang, X., G. A. Vecchi, T. L. Delworth, K. Paffendorf, R. Gudgel, L. Jia, S. Underwood,  
665 and F. Zeng, 2015: Extreme North American winter storm season of 2013/14:  
666 Roles of radiative forcing and the global warming hiatus 9in “Explaining Extremes  
667 of 2014 from a Climate Perspective”] *Bull. Amer. Meteor. Soc.*, 96(12), S25-S28.

668 Yonekura, E., and T. M. Hall, 2014: ENSO effect on East Asian tropical cyclone  
669 landfall via changes in tracks and genesis in a statistical model. *J. Appl. Meteorol.*  
670 *Clim.*, **53**, 406-420.

671

672 **Fig 1:** ETC tracks 1979-2015 whose intensity (local SLP climatology minus central  
673 pressure) reach at least 35mb. Tracks are color coded by intensity: any intensity  
674 (blue), greater than 30mb (yellow), and greater than 50mb (red). There are 1782  
675 tracks. Light blue circles indicate evaluation regions of 200km radius about the  
676 following nine cities used in figures below: New York, Boston, Washington DC,  
677 Toronto, Chicago, Detroit, Duluth, Montreal, and Halifax.

678

679 **Fig 2:** Monthly histograms of 1979-2015 ETCs in the full set (purple), minus tropical  
680 cyclones (blue), and ETCs whose intensity somewhere reaches at least 35mb (red).

681

682 **Fig 3:** Space-date kernel density formation pdf of ETCs that have 35mb+ intensity  
683 somewhere during their lifetime. The pdf is used to place simulated ETC formation

684 events in the year. It has time interval of pentads, and fields at central pentads of the  
685 months are shown. The contours are in units of counts per pentad per  $1^\circ$ -by- $1^\circ$   
686 longitude-latitude box.

687

688 **Fig 4:** Illustration of the model's track component: a four-day mean track for Jan 15  
689 conditions (red) released from  $72^\circ\text{W}$ ,  $36^\circ\text{N}$ ; and a set of 1000 track simulations  
690 including the stochastic component (gold) released from the same point. Also shown  
691 are historical tracks originating from within 175km of  $72^\circ\text{W}$ ,  $36^\circ\text{N}$ . In the  
692 simulations  $\text{NAO} = -0.4$  and  $\text{ENSO} = -0.3$ , the mean standardized anomaly values for  
693 historical ETC originating from the 175km-radius region.

694

695 **Fig 5:** Example of intensity time series sampling. Left: A historical target track on  
696 which to place an intensity series, selected from 2012 (blue), the sub-set of tracks  
697 from 1979-2015 excluding 2012 that have at least a 0.001 sampling probability  
698 according to the track-similarity criteria (thin red), and the most probable track  
699 (thick red). For this example the most probable track has a selection probability of  
700 0.45, while the next three highest probabilities are 0.23, 0.20, and 0.04. Right: The  
701 intensity time series that correspond to the tracks, plotted versus day from  
702 formation, including the most likely sampled (thick red) and the out-of-sample  
703 historical (blue) for comparison. The sampled series have been scaled in time to  
704 match the duration of the target track.

705



706 **Fig 6:** Four simulations of 1979-2015 colored coded by intensity: all tracks (blue),  
707 30mb+ (yellow), and 50mb+ (red).

708

709 **Fig. 7:** Three examples of simulated ETCs more extreme than any ETC occurring in  
710 the 1979-2015 historical record. They pass within 200km of Washington DC, New  
711 York City, and Boston, as labeled, with intensity greater than 60mb. Color intervals  
712 are units of mb.

713

714 **Fig 8:** Number of 1979-2015 tracks crossing six lines of constant longitude in 5°  
715 latitude bins (left) and six lines of constant latitude in 5° longitude bins (right).  
716 Eastward crossing (left) is indicated by the rightward bulge and northward crossing  
717 (right) by the upward bulge. Units are counts per 5° latitude (left) and longitude  
718 (right) accumulated over 1979-2015, and the flux magnitudes are indicated by the  
719 bar lengths in the upper left of each panel. Red curves represent crossings of the  
720 historical track set. Dark blue represents the inner 90% across the ensemble of  
721 1979-2015 simulations. Vertical and horizontal dashed lines indicate zero flux and  
722 are shown for reference.

723

724 **Fig 9:** Intensity as a function of return period of ETCs whose centers pass within  
725 200km of the cities labeled here and indicated in Fig 1. The blue curves are obtained  
726 directly from the 1979-2015 historical data, the orange curves indicate the 5% and  
727 95% across 1000 simulations of 1979-2015. Red is obtained from placing the 1000  
728 simulations in series, resulting in a 37,000-year simulation.

729

730 **Fig 10:** Annual rate of an ETC with 50mb+ intensity passing within 200km as a  
731 function of ENSO and NAO as labeled in standardized units. Contour units are yr<sup>-1</sup>.

732

733 **Fig 11:** Fractional change in annual rate of an ETC with 50mb+ intensity passing  
734 within 200km compared to the neutral state as a function of ENSO and NAO as  
735 labeled. Contours are fractional difference from the neutral state. Values are plotted  
736 only where the annual rate is greater than 0.01.

737

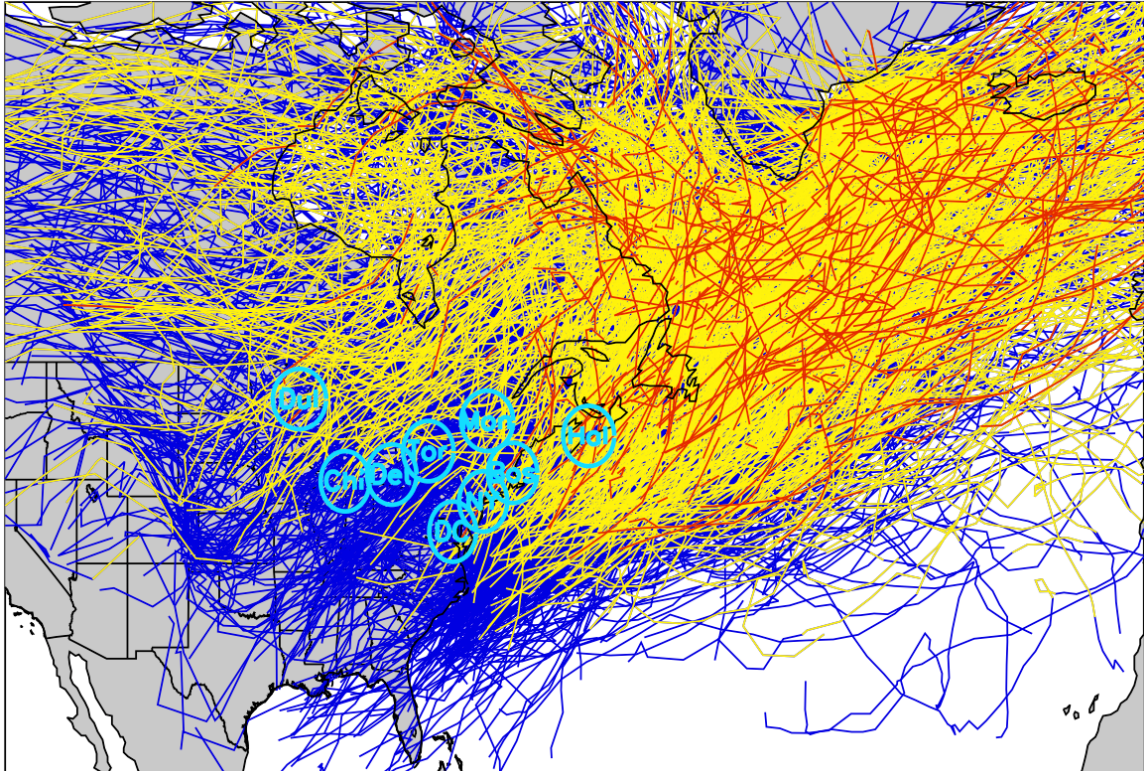
738 **Fig 12:** Formation rate ratios of the specified ENSO-NAO state to the neutral state  
739 for Jan 15. Values are plotted only where the rate is greater than 5% of its  
740 geographic maximum. Contours are fractional difference from the neutral state.

741

742 **Fig 13:** Mean tracks (track simulations without the stochastic component) have  
743 identical fixed durations of four days originating from three locations at nine ENSO-  
744 NAO states for Jan 15. In each panel red curves represent the mean tracks for the  
745 specified ENSO-NAO state, and blue curves represent the neutral state shown for  
746 reference.

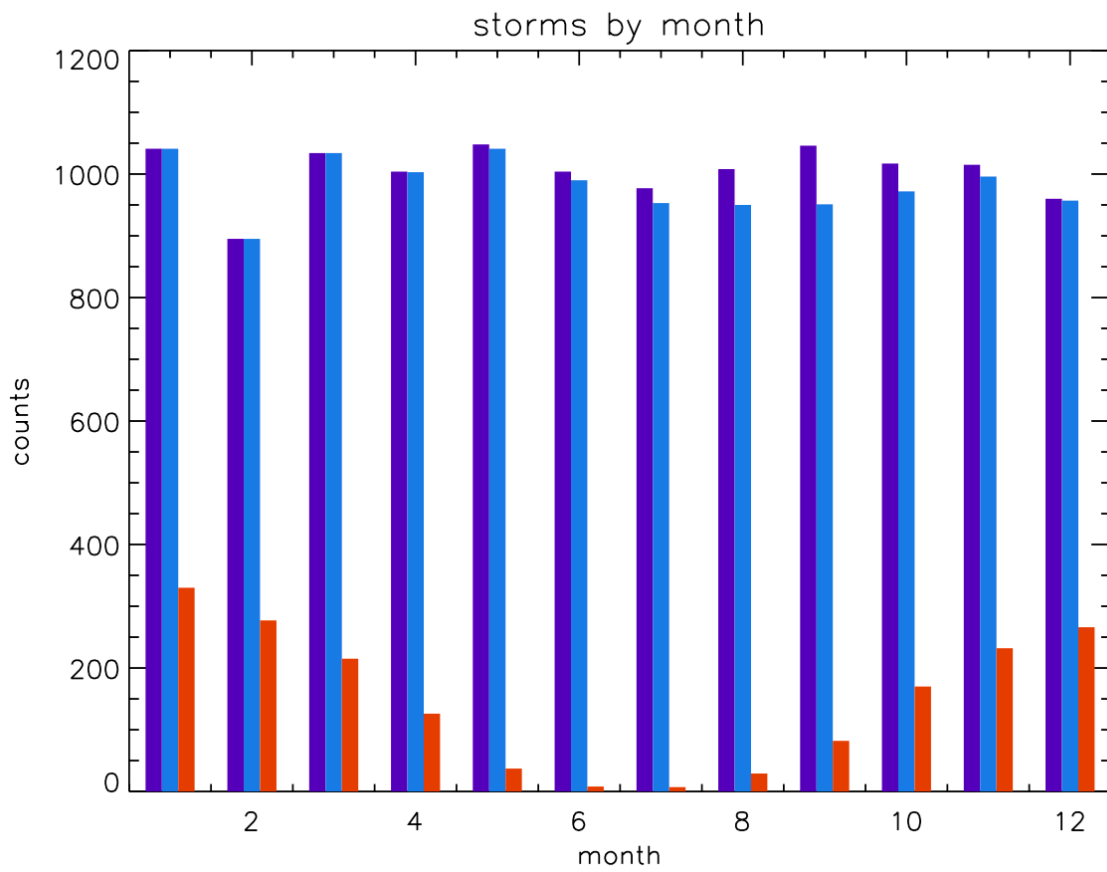
747

748 **Fig 14:** Annual occurrence rate of an ETC with 50mb+ intensity within 200km of  
749 New York City (left) and Duluth MN (right) as functions of ENSO and NAO. The  
750 minimum to maximum range for New York City is 0.012-0.05 yr<sup>-1</sup> and for Duluth is  
751 0.004-0.03 yr<sup>-1</sup>.



752

753 **Fig 1:** ETC tracks 1979-2015 whose intensity (local SLP climatology minus central  
754 pressure) reach at least 35mb. Tracks are color coded by intensity: any intensity  
755 (blue), greater than 30mb (yellow), and greater than 50mb (red). There are 1782  
756 tracks. Light blue circles indicate evaluation regions of 200km radius about the  
757 following nine cities used in figures below: New York, Boston, Washington DC,  
758 Toronto, Chicago, Detroit, Duluth, Montreal, and Halifax.

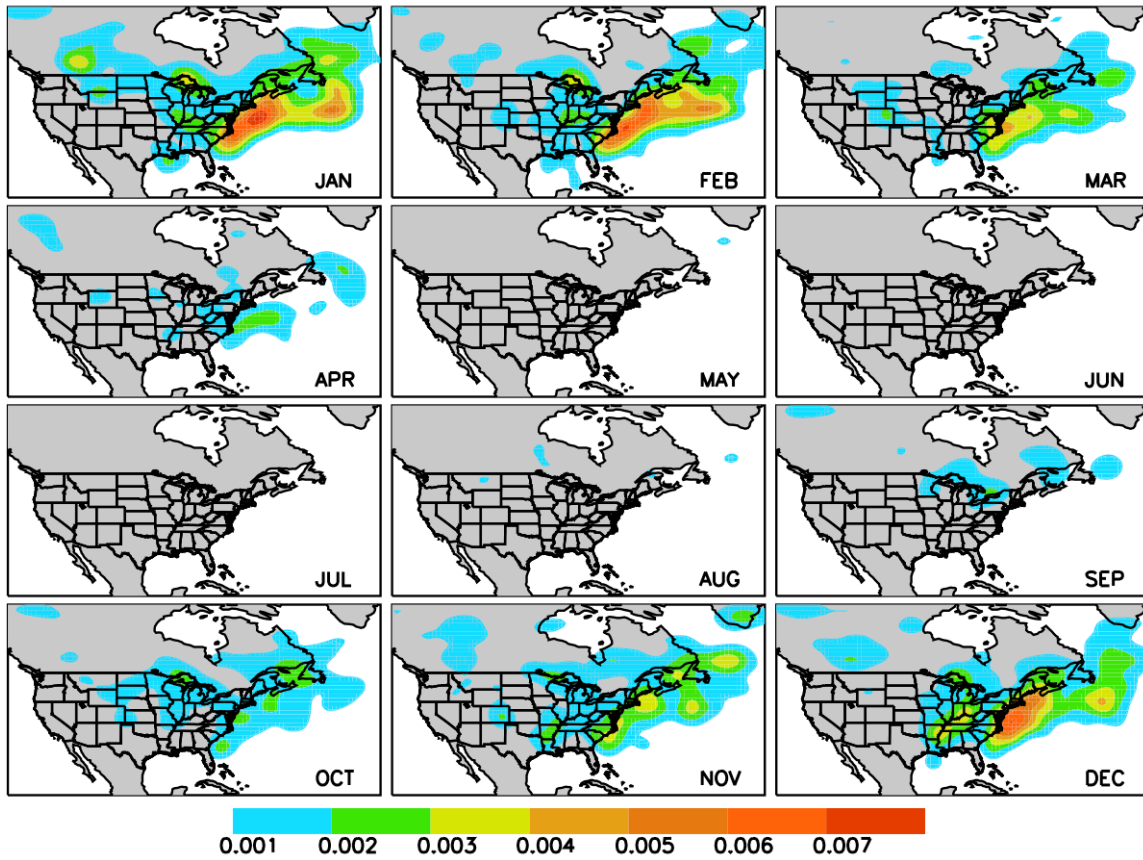


759

760

761 **Fig 2:** Monthly histograms of 1979-2015 ETCs in the full set (purple), minus tropical  
 762 cyclones (blue), and ETCs whose intensity somewhere reaches at least 35mb (red).

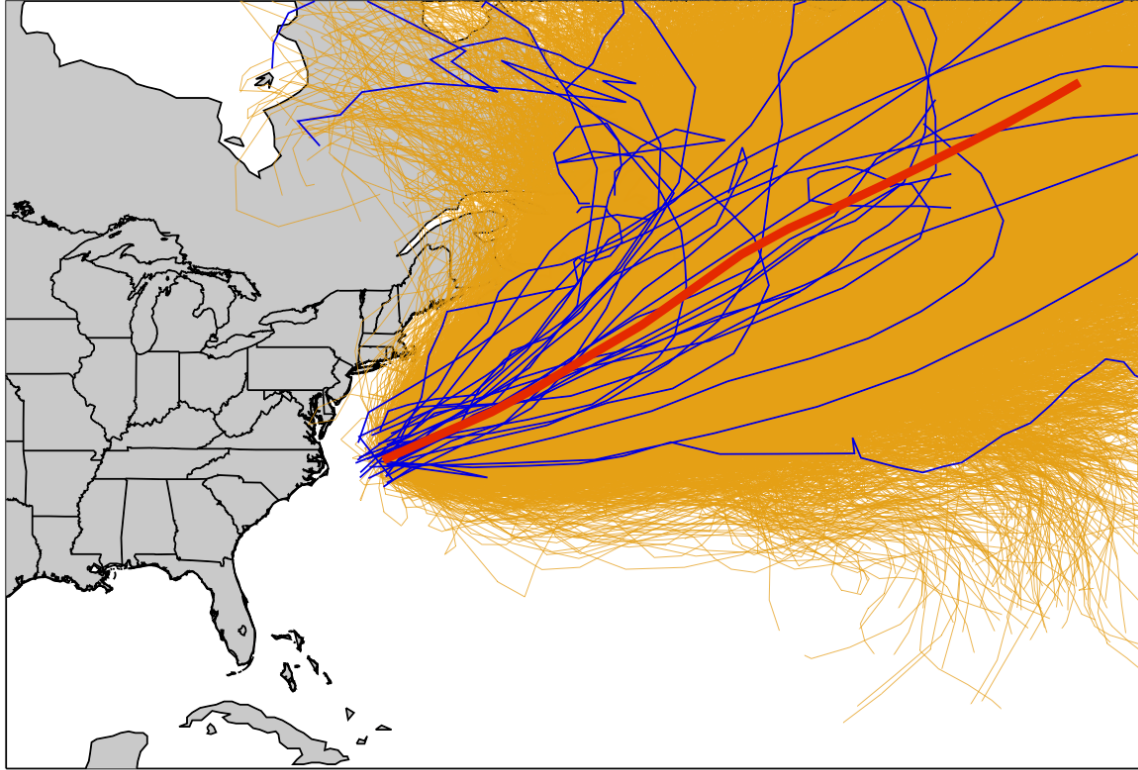
763



764

765

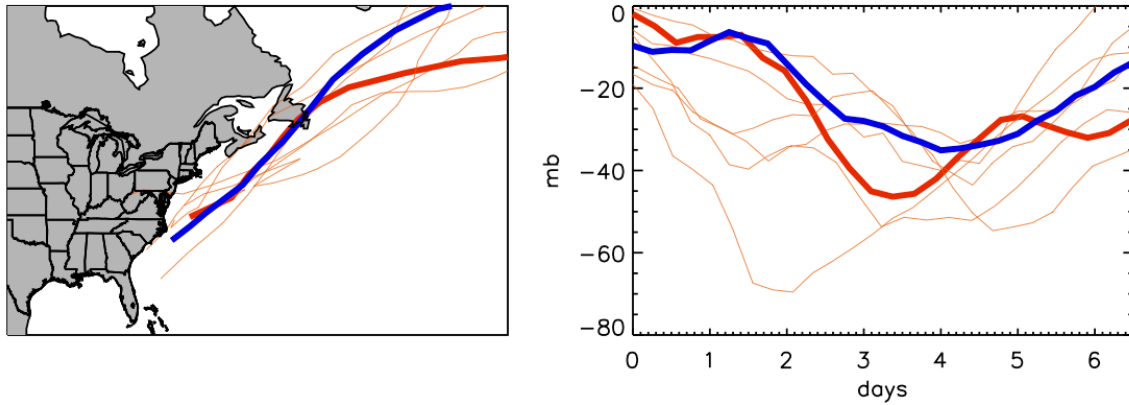
766 **Fig 3:** Space-date kernel density formation pdf of ETCs that have 35mb+ intensity  
 767 somewhere during their lifetime. The pdf is used to place simulated ETC formation  
 768 events in the year. It has time interval of pentads, and fields at central pentads of the  
 769 months are shown. The contours are in units of counts per pentad per 1°-by-1°  
 770 longitude-latitude box.



771

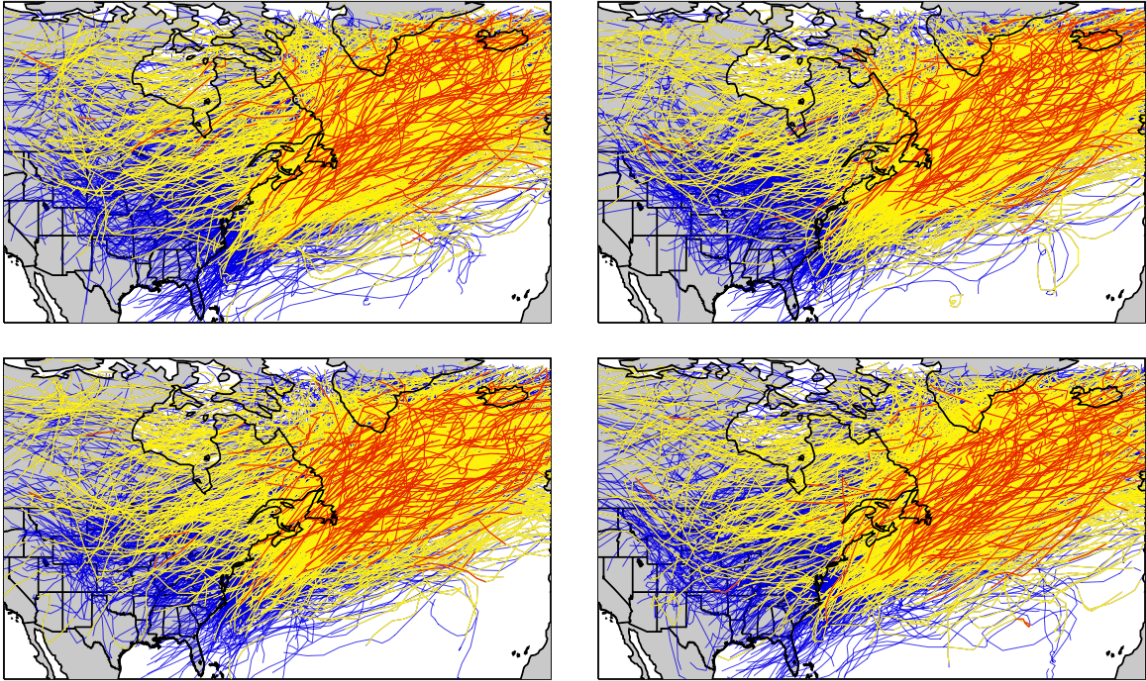
772 **Fig 4:** Illustration of the model's track component: a four-day mean track for Jan 15  
773 conditions (red) released from 72°W, 36°N; and a set of 1000 track simulations  
774 including the stochastic component (gold) released from the same point. Also shown  
775 are historical tracks originating from within 175km of 72°W, 36°N. In the  
776 simulations NAO = -0.4 and ENSO = -0.3, the mean standardized anomaly values for  
777 historical ETC originating from the 175km-radius region.

778



779

780 **Fig 5:** Example of intensity time series sampling. Left: A historical target track on  
 781 which to place an intensity series, selected from 2012 (blue), the sub-set of tracks  
 782 from 1979-2015 excluding 2012 that have at least a 0.001 sampling probability  
 783 according to the track-similarity criteria (thin red), and the most probable track  
 784 (thick red). For this example the most probable track has a selection probability of  
 785 0.45, while the next three highest probabilities are 0.23, 0.20, and 0.04. Right: The  
 786 intensity time series that correspond to the tracks, plotted versus day from  
 787 formation, including the most likely sampled (thick red) and the out-of-sample  
 788 historical (blue) for comparison. The sampled series have been scaled in time to  
 789 match the duration of the target track.



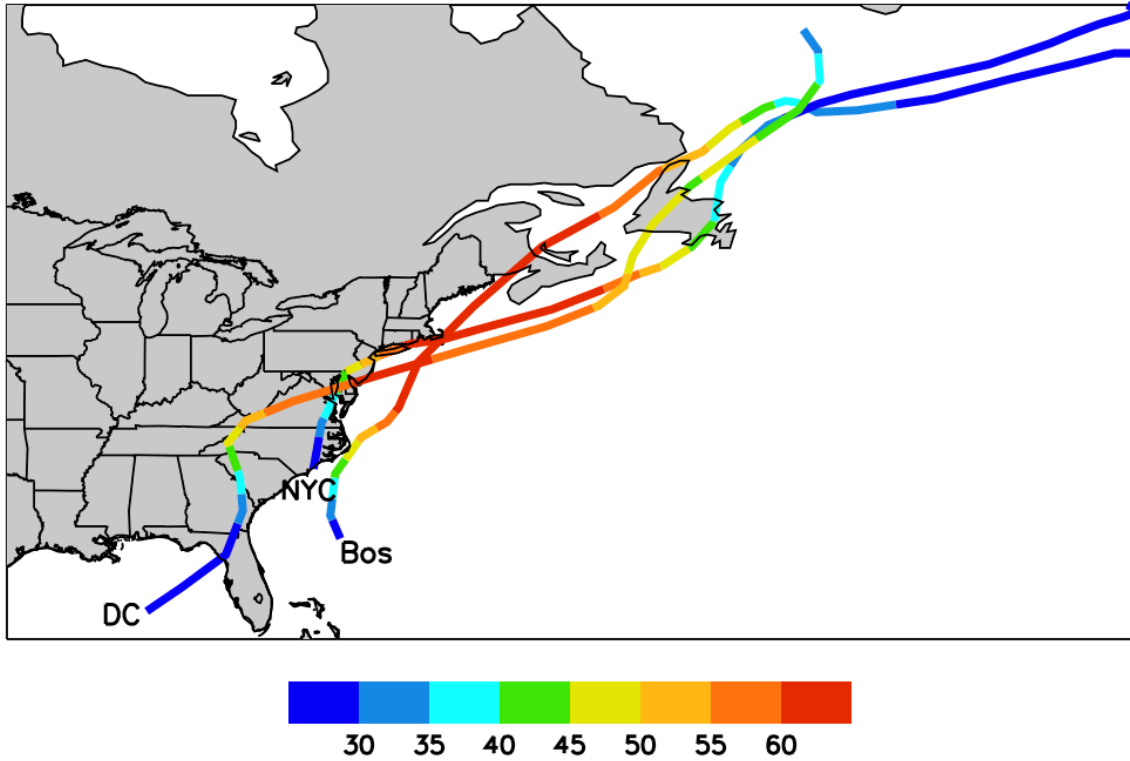
790

791 **Fig 6:** Four simulations of 1979-2015 colored coded by intensity: all tracks (blue),

792 30mb+ (yellow), and 50mb+ (red).

793



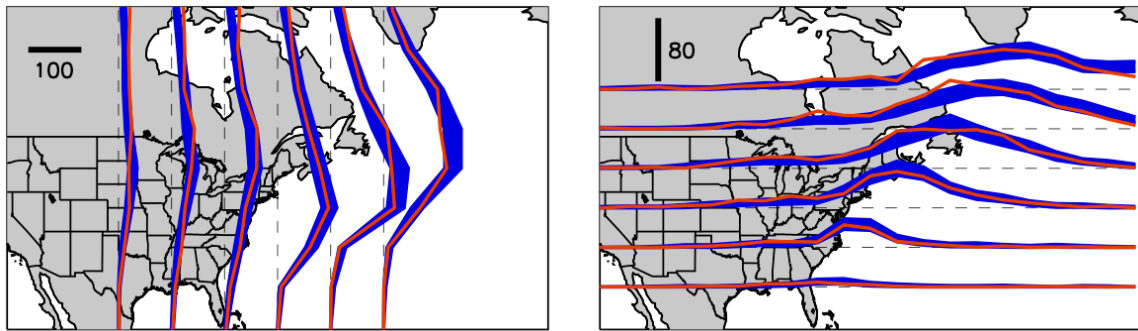


794

795 **Fig. 7:** Three examples of simulated ETCs more extreme than any ETC occurring in  
 796 the 1979-2015 historical record. They pass within 200km of Washington DC, New  
 797 York City, and Boston, as labeled, with intensity greater than 60mb. Color intervals  
 798 are units of mb.

799

800



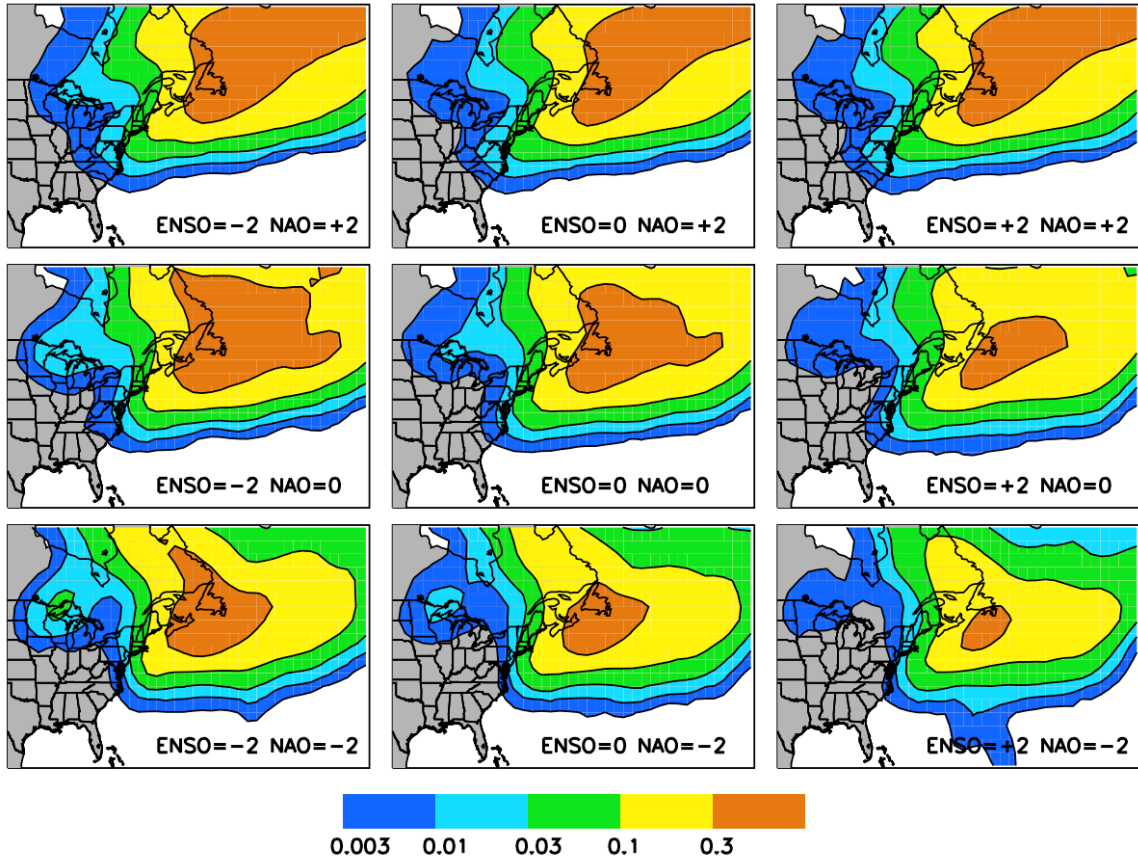
801

802 **Fig 8:** Number of 1979-2015 tracks crossing six lines of constant longitude in  $5^\circ$   
803 latitude bins (left) and six lines of constant latitude in  $5^\circ$  longitude bins (right).  
804 Eastward crossing (left) is indicated by the rightward bulge and northward crossing  
805 (right) by the upward bulge. Units are counts per  $5^\circ$  latitude (left) and longitude  
806 (right) accumulated over 1979-2015, and the flux magnitudes are indicated by the  
807 bar lengths in the upper left of each panel. Red curves represent crossings of the  
808 historical track set. Dark blue represents the inner 90% across the ensemble of  
809 1979-2015 simulations. Vertical and horizontal dashed lines indicate zero flux and  
810 are shown for reference.



811

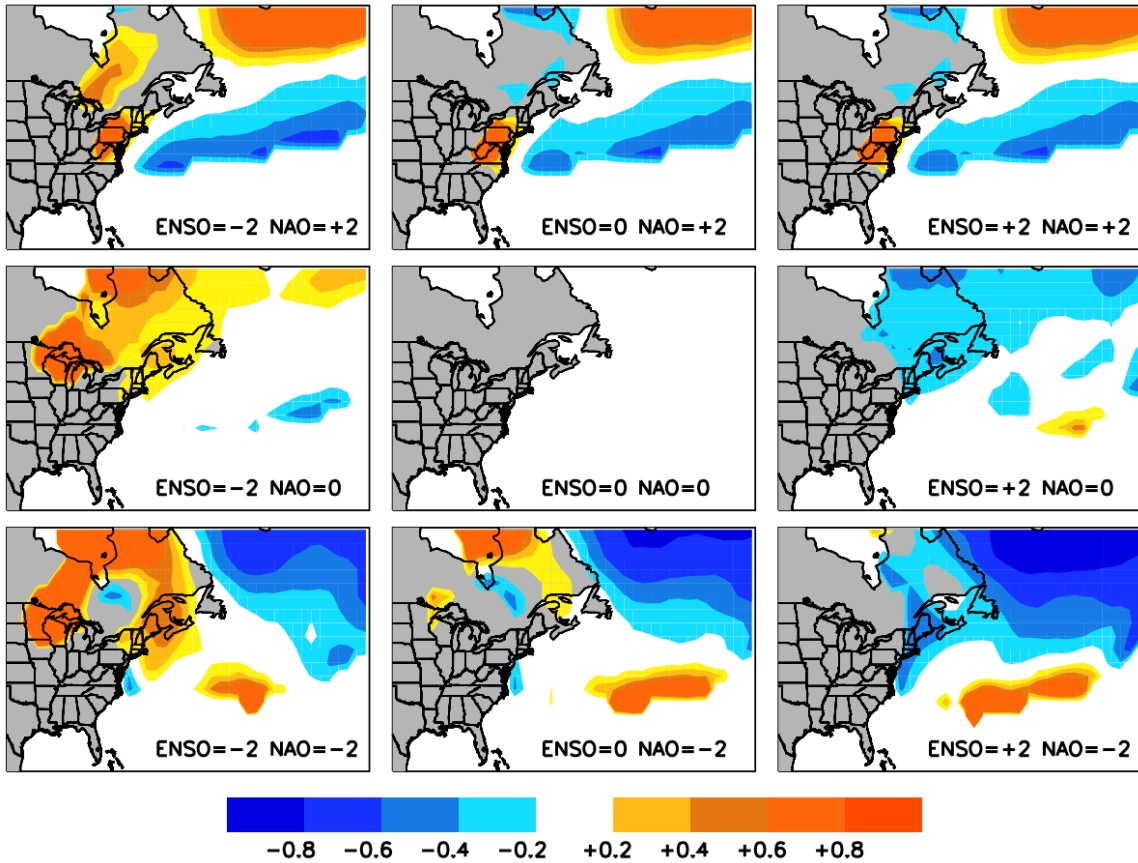
812 **Fig 9:** Intensity as a function of return period of ETCs whose centers pass within  
 813 200km of the cities labeled here and indicated in Fig 1. The blue curves are obtained  
 814 directly from the 1979-2015 historical data, the orange curves indicate the 5% and  
 815 95% across 1000 simulations of 1979-2015. Red is obtained from placing the 1000  
 816 simulations in series, resulting in a 37,000-year simulation.



817

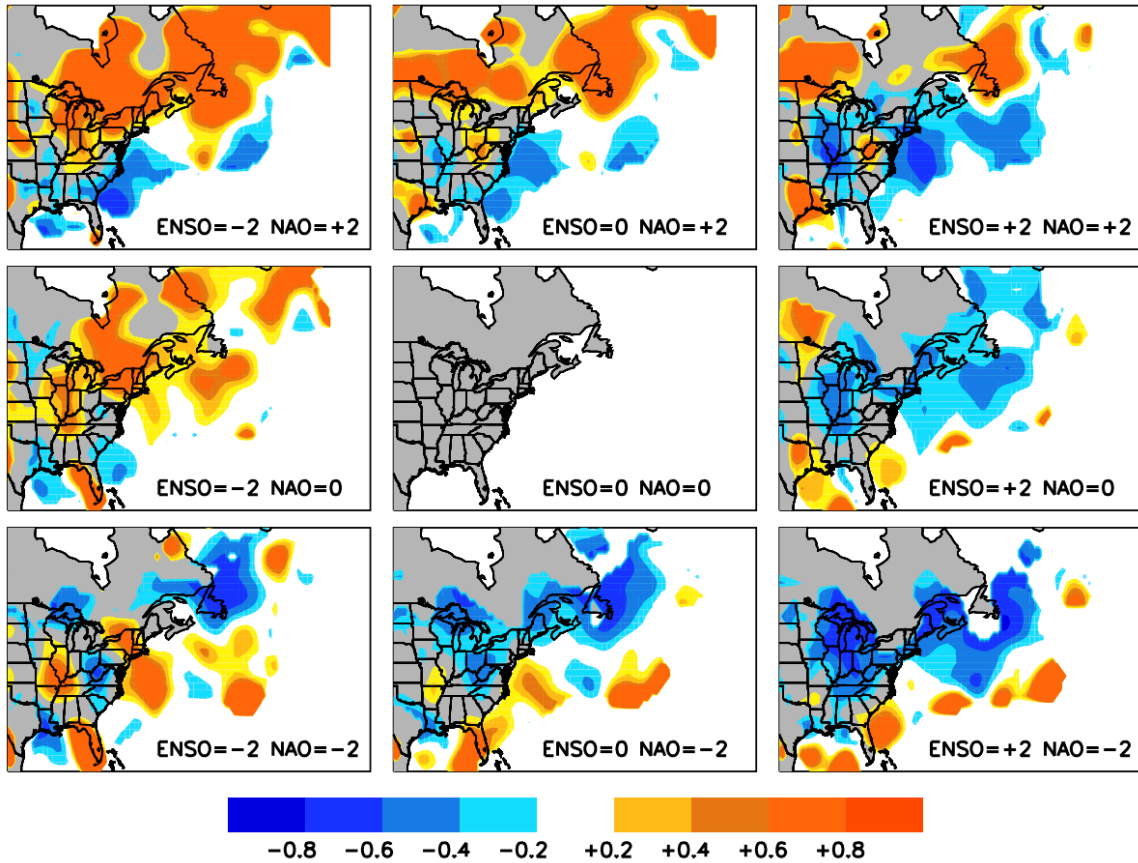
818 **Fig 10:** Annual rate of an ETC with 50mb+ intensity passing within 200km as a  
 819 function of ENSO and NAO as labeled in standardized units. Contour units are yr<sup>-1</sup>.

820



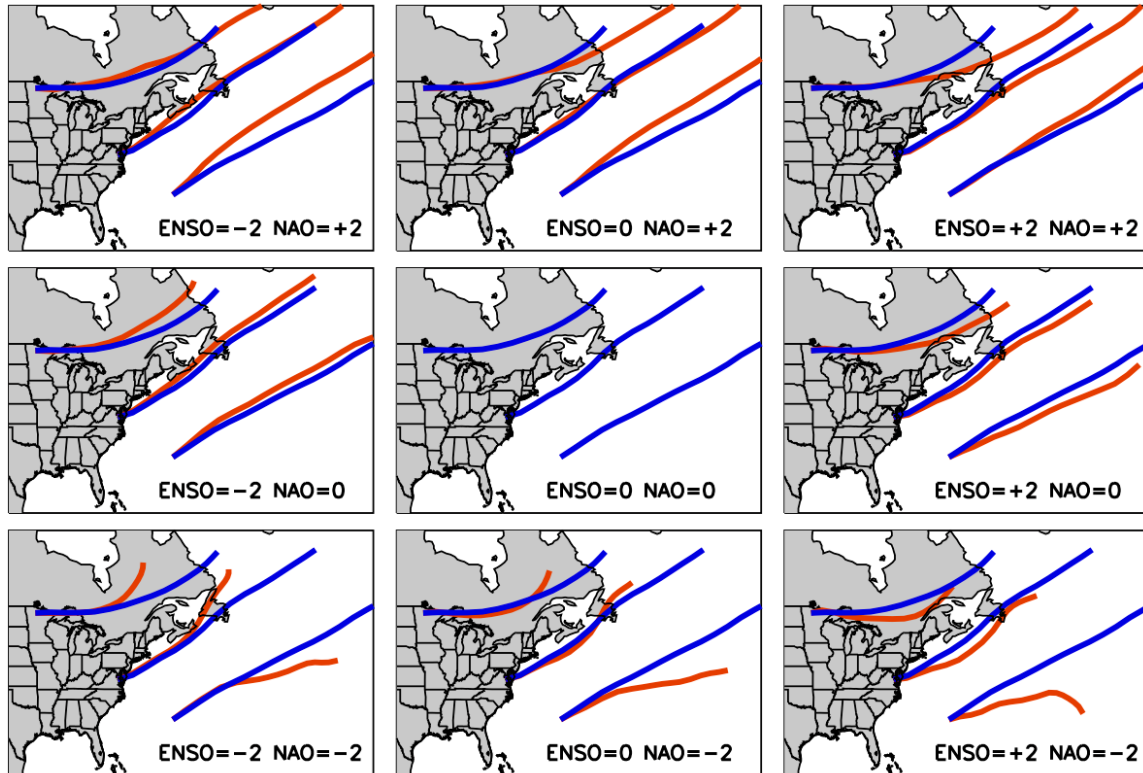
821

822 **Fig 11:** Fractional change in annual rate of an ETC with 50mb+ intensity passing  
 823 within 200km compared to the neutral state as a function of ENSO and NAO as  
 824 labeled. Contours are fractional difference from the neutral state. Values are plotted  
 825 only where the annual rate is greater than 0.01.



826

827 **Fig 12:** Formation rate ratios of the specified ENSO-NAO state to the neutral state  
 828 for Jan 15. Values are plotted only where the rate is greater than 5% of its  
 829 geographic maximum. Contours are fractional difference from the neutral state.

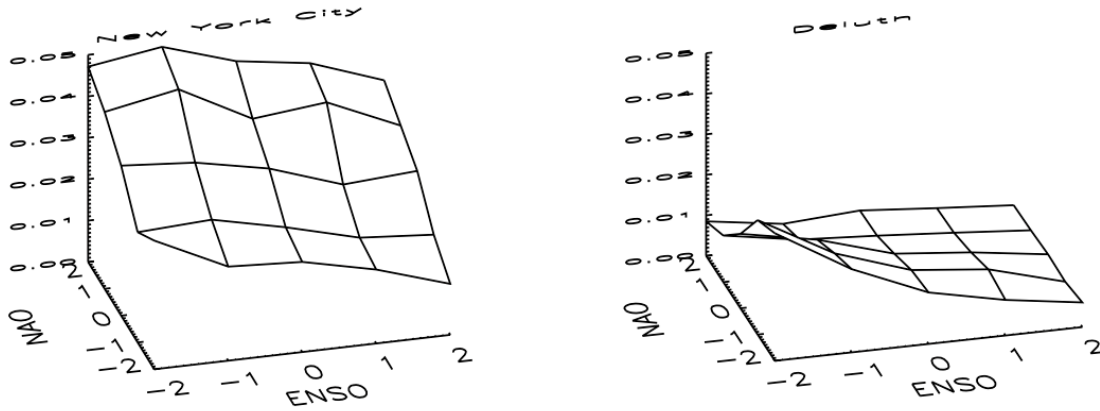


830

831 **Fig 13:** Mean tracks (track simulations without the stochastic component) have  
 832 identical fixed durations of four days originating from three locations at nine ENSO-  
 833 NAO states for Jan 15. In each panel red curves represent the mean tracks for the  
 834 specified ENSO-NAO state, and blue curves represent the neutral state shown for  
 835 reference.

836

837



838

839 **Fig 14:** Annual occurrence rate of an ETC with 50mb+ intensity within 200km of  
840 New York City (left) and Duluth MN (right) as functions of ENSO and NAO. The  
841 minimum to maximum range for New York City is 0.012-0.05 yr<sup>-1</sup> and for Duluth is  
842 0.004-0.03 yr<sup>-1</sup>.

843

844